GEORGIA INSTITUTE OF TECHNOLOGY — OFFICE OF CONTRACT ADMINISTRATION

PROJECT ADMINISTRATION DATA SHEET

[x] ORIGINAL [ ] REVISION NO. _____

Project No. E-25-661 DATE 7/1/82

Project Director: Dr. Ward Winer School/~~Lab~~ Mechanical Eng.

Sponsor: International Business Machines, Corporation

Type Agreement: Agreement No. S ON49850

Award Period: From 6/21/82 To ~~10/20/82~~ 4/30/83 (Performance) 10/20/82 (Reports)

Sponsor Amount: $22,000 Contracted through:

Cost Sharing: _____ GTRI/~~GIT~~

Title: Exploratory Study of Infrared Measurement of Magnetic Tape/Head Contact Temperatures

ADMINISTRATIVE DATA

OCA Contact Faith G. Costello

1) Sponsor Technical Contact:

Dr. Bharat Bhushan
~~Advisory Engineer, MG: 75B/061-1~~
International Business Machines Corp.
General Products Division
Tucson, Arizona ~~85744~~ 5580 So. Nogales Hwy. Bldg. 005
85706

2) Sponsor Admin/Contractual Matters:

A. R. Lundeberg
Contract Administrator, Dept. 34H/040-1
International Business Machines Corp.
General Products Division
Tucson, Arizona 85744

(602) 741-5000

Defense Priority Rating: NA

Security Classification: (Industrial) see below*

RESTRICTIONS

See Attached NA Supplemental Information Sheet for Additional Requirements.

Travel: Foreign travel must have prior approval — Contact OCA in each case. Domestic travel requires sponsor approval where total will exceed greater of $500 or 125% of approved proposal budget category.

Equipment: Title vests with sponsor

COMMENTS:

*Prior written approval from IBM is necessary to, in any manner, "advertise, publish or otherwise disclose the fact that (GTRI) has furnished or contracted to furnish to IBM, the material and services ordered hereunder".

COPIES TO:

Administrative Coordinator
Research Property Management
Accounting
Procurement/EES Supply Services
Research Security Services
~~Reports Coordinator (OCA)~~
Legal Services (OCA)
Library
EES Public Relations
Computer Input
Project File
Other GTRI

FORM OCA 4:78

GEORGIA INSTITUTE OF TECHNOLOGY OFFICE OF CONTRACT ADMINISTRATION

SR284 81

SPONSORED PROJECT TERMINATION SHEET

Date August 16, 1983

Project Title: Exploratory Study of Infrared Measurement of Magnetic Tape/Head Contact Temperatures

Project No: E-25-661

Project Director: Dr. Ward Winer

Sponsor: International Business Machines Corporation

Effective Termination Date: 4/30/83

Clearance of Accounting Charges: _____

Grant/Contract Closeout Actions Remaining:

- [X] Final Invoice and Closing Documents
- [ ] Final Fiscal Report
- [ ] Final Report of Inventions
- [ ] Govt. Property Inventory & Related Certificate
- [ ] Classified Material Certificate
- [ ] Other _____

Assigned to: Mechanical Engineering (School/~~Laboratory~~)

COPIES TO:

Administrative Coordinator	Research Security Services	EES Public Relations (2)
Research Property Management	Reports Coordinator (OCA) ✓	Computer Input
Accounting	Legal Services (OCA)	Project File
Procurement/EES Supply Services	Library	Other _____

OCA Support Services
E-25-661

Georgia Institute of Technology

A UNIT OF THE UNIVERSITY SYSTEM OF GEORGIA

SCHOOL OF MECHANICAL ENGINEERING

ATLANTA, GEORGIA 30332

4 November 1982

Dr. Bharat Bhushan
Advisory Engineer
International Business Machines Corporation
General Products Division
Mail Code: 75B/061-1
Tucson, Arizona 85744

Subject: Progress Report through 21 October 1982

Dear Dr. Bhushan:

A high speed rotating disc has been assembled which can achieve speeds of 30,000 rpm corresponding to a linear velocity of 850 ft/sec. This disc will enable measurement of the response time of the IR microdetector to within 0.1 μs.

Testing has begun on the radiance vs. temperature of the magnetic tape received 6 October 82. A heating/cooling unit has been assembled which can control temperature to ± 0.1C over the range 15C-50C. To assure that the tape temperature can be recorded to within this limit, the tape is mounted onto a copper block with conductive silver paint. Just beneath the surface is embedded a T-type thermocouple with an active element length of 0.375 in.

A tape head mounting fixture with 3-component force measurement capability has been fabricated.

Delivery of the standard sapphire lenses in expected in a week. The special heads will be delayed due to the late (18 October 82) receipt of machine drawings of the head modifications at Crystal Systems.

Because of delays in the program due to delivery of lenses and tapes we are requesting a four-month extension.

If there are any questions please call.

Sincerely,

Scott Bair
Research Engineer

jv

xc: W. O. Winer
Principal Investigator

J. A. Brighton, Director
Mechanical Engineering

OCA Support Services

E-25-661

FINAL REPORT
AGREEMENT NO. SN49850

EXPLORATORY STUDY OF INFRARED MEASUREMENT OF MAGNETIC TAPE/HEAD CONTACT TEMPERATURES

Prepared by:

R. GULINO
Graduate Research Assistant
S. BAIR
Research Engineer
W. O. WINER
Professor

Prepared for:

INTERNATIONAL BUSINESS MACHINES CORPORATION
General Products Division
Tucson, Arizona 85744

April 1983

GEORGIA INSTITUTE OF TECHNOLOGY
A UNIT OF THE UNIVERSITY SYSTEM OF GEORGIA
SCHOOL OF MECHANICAL ENGINEERING
ATLANTA, GEORGIA 30332

1983

THE MEASUREMENT OF TEMPERATURES OF MICROSCOPIC AREAS WITHIN A TAPE/SIMULATED TAPE HEAD INTERFACE USING INFRARED RADIOMETRIC TECHNIQUES

Submitted to:

INTERNATIONAL BUSINESS MACHINES CORPORATION

Dr. Bharat Bhushan
IRS Number 58-6002023

Prepared by:

GEORGIA INSTITUTE OF TECHNOLOGY

Ronald Gulino
Graduate Research Assistant

Scott Bair
Research Engineer

Ward O. Winer
Professor and Director
Tribology and Rheology Laboratory

April 1983

TABLE OF CONTENTS

APPENDICES Page

LIST OF TABLES

LIST OF ILLUSTRATIONS

SUMMARY

This exploratory study concerns the infrared measurement of steady-state and transient temperatures of microscopic areas within the contact region formed by a magnetic tape passing over a simulated recording head. This research demonstrates that tape surface temperature can be measured within specific limits of response time and sensitivity. Due to its high transmittivity in the relevant infrared band, sapphire was chosen as the material to be used in the fabrication of a simulated recording head. The Barnes RM2A infrared microscope was the principle radiometer used, while a best effort was made in scanning with the AGA Thermovision M50. This research effort was comprised of five main parts:

1. determination of response time, spot size, and noise characteristics of the radiometer used.

2. radiation analysis of the radiometer used in conjunction with the magnetic tape-tape head configuration.

3. determination of the radiative properties of the magnetic tape.

4. construction of a tape transport system to measure tape running condition such as speed and resultant forces acting on the tape head.

5. experimental measurements of traction versus load and temperature measurements in both the steady-state and transient modes under various running conditions.

The traction versus load characteristics of the magnetic tape-sapphire tape head interface were also observed. The high speed measurements were divided into two regimes; (1) non-contact hydrodynamic film region, and (2) tape-head contact region. The steady-state temperature measurements displayed a strong correlation with the measured traction versus load curve. Almost no temperature rise was found in the non-contact hydrodynamic film region while a temperature rise of a few degrees centrigrade was found when there was tape-head contact. Because no temperature peaks were found in the transient mode, the magnitude and/or duration of these flashes, if they exist, must be less than the sensitivity of the Barnes microscope in this mode. The

resolution in the transient mode with external filtering is on the order of 10°C. The results with the AGA Thermovision 750 were consistent with the measurements obtained with the Barnes RM2A.

The following tables summarize the measurements made with the Barnes RM2A microscope.

TEMPERATURE MEASUREMENTS

Steady-State
(15x Objective)
Instrument Response Time 0.5/sec

Tape Running Conditions			Measured Temperature Rise above Ambient	Error Interval
Speed (m/s)	Load (N)	Run Time (minutes)	(°C)	
3.82	0.7*	0.5	0.0	0.6**
3.82	1.1*	0.5	0.5	0.6**
3.82	2.4*	0.5	3.2	0.5
3.82	2.6*	0.5	3.5	0.5
0.32	0.6	1.0	0.4	0.5
0.32	1.2	1.0	1.0	0.5
0.32	1.7	1.0	1.1	0.5

*measured at peak load at the end of load transient
**non-contact film region

Transient
Instrument Response Time 7.8 μsec

Instrument Spot Size (μm)	Tape Running Conditions Speed (m/s)	Load (N)	Temperature Rise Above Ambient (°C)	Error Interval (°C)
124**	3.82	0.7 - 1.8	*	9
124**	0.32	0.5 - 1.8	*	9
86***	3.82	0.7 - 1.8	*	13
86***	0.32	0.5 - 1.8	*	13

*No signal greater than the error interval was observed.
**15x objective
***36x objective

CHAPTER I

INTRODUCTION

The purpose of this study was to explore the feasibility of measuring the temperature of microscopic areas within the interface formed by passing a magnetic tape over a simulated recording head. All materials emit radiation which depends upon the surface temperature of the material. To quantitatively determine the temperature, the radiative characteristics of the materials as well as the radiant heat transfer properties of the particular geometrical configuration must be known. Once these factors have been computed or measured, the temperature may be deduced from the output of the radiometer. Due to the larger spot size and slower response of the AGA Thermovision 750, the Barnes RM2A infrared microscope was the principal radiometer used.

This report is divided into the four main sections:

1. Infrared measurement system,
2. Tape drive system,
3. Experimentation, and
4. Conclusions.

The infrared measurement system section presents the determination of the tape radiative properties, determination of the limitations of the radiometer, and formulation or a radative analysis which explicitly relates the output signal to the tape temperature. The tape drive section consists of an explanation of the instrumentation used in controlling the tape tension, speed and position within the contract specifications. The experimentation section encompasses three main areas:

1. traction vs. load,
2. steady state temperatures,
3. transient temperatures.

The final section outlines areas for further investigations, correlation of experimental results, and suggests possible explanations for these results.

CHAPTER II

INFRARED MEASUREMENT SYSTEM

BARNES RM2A INFRARED MICROSCOPE

The Barnes RM2A infrared microscope is a highly sensitive high resolution microscope which measures the infrared energy naturally radiated by all objects. The spot size, response time, and noise characteristics of this device will be explored in this chapter. The spot size refers to the actual area over which infrared radiation is collected. Thus the temperature derived from this signal corresponds to an average temperature taken over the spot area. The rise time is defined as the time required for the device output signal to reach 63% of its ultimate value after receiving a step input. The noise characteristics refers to the peak-to-peak noise interval around a constant signal. After the radiometric characteristics of this device are discussed, the operating equation will be introduced.

The operating equation allows the target temperature to be deduced from the output signal. The operating equation for the experimental set-up to determine the tape radiative properties will be introduced. The procedure for determining the tape radiative properties; emissivity, reflectivity, and transmittivity; will be discussed and subsequently a table of the measured values will be presented.

Spot Size

The minimum spot size for each objective with air as the transmitting medium was determined by Barnes Engineering. The spot size must be adjusted for the presence of the sapphire in the optical path. The following derivation relates the shift of the object plane for a given sapphire thickness [Figure 2.1].

Using Snell's law

$$n_o \sin\phi_o = n_1 \sin\phi_1 \qquad (2.1)$$

From the definition of tangent

$$\text{Tan } \phi_o = \frac{\beta}{\sigma} \quad ; \quad \tan \phi_1 = \frac{\beta}{t}$$

Applying paraxial ray theory

$$\sin \phi_o = \frac{\beta}{\sigma} \quad ; \quad \sin \phi_1 = \frac{\beta}{t} \qquad (2.2)$$

Upon substitution of (2.2) into (2.1)

$$\zeta = \frac{t(n_1 - n_o)}{n_1}$$

where $\zeta \equiv$ shift in the object plane.

Using the shift in the object plane, the sapphire thickness, the limiting angle of the acceptance (one of each objective), and the spot size of the objective in air, the spot size on the surface contacting the tape can be calculated [Figure 2.2].

Let

D = Diameter of the aperture stop (objective opening diameter)

F = working distance

Then

$$\tan \theta_o = \frac{D/2 - D_1/2}{F} \quad \text{Definition of Tangent} \qquad (2.3)$$

$$\tan \theta_o = \frac{\alpha - D_1/2}{t - \delta} \qquad (2.4)$$

$$\tan \theta_1 = \frac{\alpha - D_2/2}{t} \qquad (2.5)$$

$$n_o \sin \theta_o = n_o \sin \theta_1 \quad \text{Snell's Law} \qquad (2.6)$$

Substitution of (2.4) into (2.3) and solving for α

$$\alpha = (t-\delta) \frac{(D - D_1)}{2F} + \frac{D_1}{2} \qquad (2.7)$$

solving equation (2.5) for D_2

$$D_2 = 2(\alpha - t(\tan \theta_1)) \qquad (2.8)$$

Using Equation 2.3 with Equation 2.7 to obtain tan θ.

$$\tan \theta_1 = \tan \left(\text{Arcsin } \frac{n_o}{n_1} \sin \text{ artan } \frac{(D-D_1)}{2F}\right. \qquad (2.9)$$

Now computing α, tan θ, in equation (2.5) and (2.7) enables the computation of D_2 from equation (2.6). The spot size is substantially (~4X) times) increased as shown in Table 2.1.

DETERMINATION OF DETECTOR RESPONSE TIME

To determine the response time of the detector, a variable speed chopper was built. The chopper consisted of a notched rotating disk which was driven by a gear box attached to a digitally controlled motor [Figure 2.3]. Large rotational speeds were used so that the detector spotsize would be crossed in a very short time (e.g., < 5% of the response time). A Nicolet digital oscilloscope was used to record the signals from the Barnes infrared microscope. The response time was calculated as the time required to reach 63% of the signal height. The response time was measured for the A-C transient mode, the natural decay for the A-C transient mode, and for the D.C. mode with the narrow filter. The average response time in the A.C. mode was 7.75 μ seconds $\pm$ 0.7 μ sec. The error interval cited is composed of the time for the edge to cross the objective spotsize (0.2 μ seconds) in addition to the time between samplings by the Nicolet digital oscilloscope (0.5 μ seconds). The numerical values of the A.C. mode rise time, AC mode decay time, and DC-mode with narrow filter decay time are shown in Table 2.2 and

actual scan for each case are displayed in Figures 2.4, 2.5, and 2.6 respectively.

TEMPERATURE ERROR INTERVAL

The temperature error interval is determined by measuring the peak-to-peak noise in a specific operational mode and determining the temperature difference required to produce such a variation. Thus the temperature error interval is dependent on the base temperature at which the difference is measured and the effective emissivity of the target. The temperature error interval is calculated by first experimentally determining the peak-to-peak noise voltage while observing a constant signal. This result is next converted to radiance units by multiplication by a calibration constant and convection to a black body radiance scale by dividing by the surfaces effective emissivity. A base temperature is chosen and the black body radiance is found by consulting the black body radiance versus temperature curve supplied by Barnes Engineering for the RM2A microscope [Appendix B]. The radiance value computed from the noise characteristics of the specific mode is then added to the black body radiance at the base temperature. This new black body radiance level corresponds to a higher black body temperature as determined by the calibration curve supplied by Barnes Engineering. The difference in these temperatures is the temperature error interval. The following example serves to illustrate this calculation.

BARNES RM2A INFRARED MICROSCOPE - DC MODE WITH NARROW FILTER

Peak to Peak Noise = 5.5 mV

Calibration Constant $(K")^{-1}$

for 15x objective - -mode $= 0.00619 \ \frac{mW/cm^2 \cdot sr}{mV}$

Effective Surface Emissivity $= 0.7$

Base Temperature $= 20°C$

Black Body Radiance @20°C $= 3.0 \ mW/cm^2 \cdot sr$

$$\text{Blackbody radiance for noise interval} = \frac{5.5\ \text{mV}}{1} \frac{0.00619\ \text{mW/cm}^2 \cdot \text{sr}}{\text{mV}} \cdot \frac{1}{0.7}$$

$$= 0.049\ \text{mW/cm}^2 \cdot \text{sr}$$

$$\text{New black body radiance above base temperature} = 3.049\ \text{mW/cm}^2 \cdot \text{sr}$$

$$\text{Equivalent temperature, T} = 20.5°\text{C}$$

$$\text{Temperature error interval} = \Delta T = 20.5°\text{C} - 20.0°\text{C}$$

$$= 0.5°\text{C}$$

Thus the error temperature interval for a surface with effective emissivity of 0.7 at base temperature 20°C in the D.C. mode with the narrow filter is 0.5°C. Figure 2.7 is a trace of the signal in the D.C. mode with the narrow filter while viewing a constant temperature source. The peak to peak noise interval is 5.5 millivolts.

DETERMINATION OF TAPE RADIATIVE PROPERTIES

A procedure to determine the radiative characteristics of the magnetic tapes supplied using the Barnes RM2A infrared microscope was developed. The specific characteristics to be measured were the tape emissivity and reflectivity as functions of temperature and the tape transmittivity at room temperature. The experimental apparatus consisted of a means to control the temperature of the tape and use of the Barnes RM2A to measure the infrared radiation collected from the tape surface.

The temperature of the tape was controlled by attaching the tape to a copper block whose temperature was controlled by a thermoelectric heater/cooler device. Embedded at the surface of the copper block was a T-type thermocouple which measured the average surface temperature over a 9mm long line. The line ran diagonally beneath the tape at the area where the radiation was collected. A thin film of silver paint was used to thermally bond the tape to the copper block. The tape, once placed on the upper block with the magnetic side up, had one half of its surface sprayed with 3M C-110 velvet black paint (emissivity = 0.995).

The temperature of the tape was varied by controlling the the electric power in the thermoelectric device. This system resulted in control of the tape temperature over a 50°C to 15°C temperature range and creating a black body source (the painted tape) which had the same temperature as the actual tape (uncoated area).

The Barnes RM-2A infrared microscope was used to measure the radiation collected from the surface of the tape. In order to compute the radiative properties of the tape, a radiation analysis of the Barnes RM2A in conjunction with the experimental apparatus must be made. The details of this analysis is presented in the Appendix A. The operating equation for three particularly useful conditions are quoted below from Appendix A.

	Condition	Operating Equation	
1.	Surface is a Blackbody	$S_{BB} = K'' [N_T - N_E]$	(7.8)
2.	Microscope at Half Focus	$S_{\frac{1}{2}} = K'' [\varepsilon_T (N_T - N_E) - 0.12\rho_{D_T} N_E]$	(7.9)
3.	Microscope at Focus	$S = K'' [\varepsilon_T (N_T - N_E) - 0.12N_E - \rho_{ST}N_E]$	(7.10)

Definition of Symbols*

S = Signal from Barnes RM2A in millivolts

K" = Calibration constant

N = Blackbody emissive power per unit steradian at temperature T.

ε = Emissivity

ρ_S = Specular reflectivity

ρ_D = Diffuse reflectivity

Definition of Subscripts*

BB = Blackbody

½ = Half Focus

T = Tape Surface

E = Environment

*For example N_T is the blackbody emissive power per unit steradian of the magnetic tape surface at the tape surface temperature.

The radiative properties of the tape can be determined by application of these three equations. The emissivity as a function of temperature was determined by varying the tape temperature over a 50°C to 15°C interval. At a specific temperature which was recorded from the thermocouple, the radiation from the painted (blackbody) and unpainted sections of the tape were recorded at half focus by the infrared microscope. Thus the emissivity may be computed at a specific temperature as shown below.

At a specific temperature,

$$S_{BB} = K'' [N_T - N_E] \tag{7.8}$$

$$S_{\frac{1}{2}} = K'' [G_T (N_T - N_E) - 0.12\rho_{DT}N_E] \tag{7.9}$$

By dividing equation (7.9) by equation (7.8)

$$\frac{S_{\frac{1}{2}}}{S_{BB}} = \frac{K'' [\varepsilon_T (N_T - N_E) - 0.12\rho_{DT}N_E]}{K'' (N_T - N_E)}$$

Thus solving for ε_T

$$\varepsilon_T = \frac{S_{\frac{1}{2}}}{S_{BB}} + \frac{0.12\rho_{DT}N_E}{N_T - N_E} \tag{2.10}$$

For small values of ρ_{D_T} and when the tape is not at the same temperature as the environment

$$\varepsilon_T \cong \frac{S_{1/2}}{S_{BB}} \quad . \tag{2.11}$$

The emissivity of the tapes was found not to be a function of temperature in the range indicated. Based on results from the determination the radiative properties, equation (2.11) fit the data well even when the temperature of the tape was within a few degrees centigrade of the environmental temperature.

The specular reflectivity can be obtained by making measurements at a specific temperature with the microscope at full and half focus. The procedure is outlined below.

At a specific temperature

$$S_{1/2} = K'' \left[G_T(N_T - N_E) - 0.12\ \rho_{DT}\ N_E\right] \tag{7.9}$$

$$S = K'' \left[G_T(N_T - N_E) - 0.12\ \rho_{DT}\ N_E - \rho_{ST}\ N_E\right] \quad . \tag{7.10}$$

Upon subtraction of (7.9) from (7.10)

$$S - S_{1/2} = K'' \left[\rho_{ST}\ N_E\right]$$

Solving for ρ_{ST}

$$\rho_{ST} = \frac{S - S_{1/2}}{K''\ N_E} \tag{2.12}$$

The transmittivity was measured at room temperature by chopping a blockbody source at 75.0°C beneath the tape and measuring the fractional amount of transmitted radiation. The transmittivity was observed to be zero. Since there was no transmittance, Kirchoff's law may be stated in equation form as follows:

$$\rho_{D_T} + \rho_{S_T} + \varepsilon_T = 1.0 \quad .$$

This equation may be solved easily for the diffuse reflectivity. Table 2.3 summarizes the radiative properties of the three samples sent.

AGA THERMOVISION 750

The AGA Thermovision 750 is an optical scanning device which converts radiant thermal energy into an optical pattern visible on a video display screen or in terms of electronic video signals. The maximum scan rate is 2500 lines/second with 100 lines comprising one frame. The camera may be set to scan only one line at the previously quoted rate. The minimum detectable temperature rise (temperature error interval) is 0.5°C for a 20°C base temperature of emissivity 0.7. The minimum spot size with extension rings is on the order of 1.5 mm. The AGA is mainly a qualitative instrument possessing a very similar radiation analysis to that used in the Barnes RM2A infrared microscope. Due to scanning ability, the AGA enables the user to obtain information on relative temperatures and their magnitude over the whole contact region. Also the single line scan was used to search for temperature flashes over the entire width of the contact. Results from the AGA thermovision system will be discussed in a similar manner to that of the Barnes RM2A in a subsequent section.

CHAPTER III

TAPE TRANSPORT SYSTEM

A tape transport system was constructed to move the tape over a sapphire tape head through which infrared temperature measurements could be made. The Datum Data Acquisition System 120 was modified to meet the requirements specified in the contract. The principal features of this modified system were:

1. the tape contact angle could be adjusted
2. temperature measurement could be made with both the AGA Thermovision 750 and Barnes Infrared microscope
3. the tape could be run at both high and low speeds
4. the tape control had a start-stop option
5. the tension in the tape could be adjusted over a very wide range
6. the sapphire tape head was mounted with a triaxial transducer capable of measuring resultant load and traction forces
7. the tape horizontal position could be accurately controlled using a micrometer adjustment
8. the tape transport system was attached to the microscope to support uncoupled movement of the tape head and microscope

The path of the tape was extended onto an external assembly of low friction rollers. Two areas on this path were designed to enable both vertical (Barnes System) and horizontal viewing (AGA) of the tape in contact with the tape head. A slot was cut between two sets of rollers of adequate length to set the internal angle of the tape contact arc to 15°. [Figure 3.1] The tape path was modified to avoid the original tape head and tape cleaner head to eliminate the frictional heating from these contacts.

A bracket was constructed which attached the tape transport system to the base of the microscope stand. The bracket held a micrometer which enabled the tape to be repeatably positioned under the microscope. The bracket also minimized any movement of the tape head with respect to the infrared microscope.

The tape drive had two speeds. These speeds were measured by use of timing marks and the numerical values are: The tape drive system was modified to accommodate a range of loads (pressure) from 3.4 kPa (1/2 psi) to 27.6 kPa (4 psi). These pressures correspond to normal forces of 0.23 N and 1.86 N respectively. The increased tension was achieved by controlling the feedback signal to the spool motors. Adjustment was achieved by using turnbuckles to position the tension feedback levers of the tape transport system. The load was measured by a transducer placed in the mounting bracket of the tape head.

A triaxial force transducer was placed in the mounting bracket of the tape head. The output of the transducer was coupled to a charge amplifier whose output was monitored by a strip recorder. The calibration constants relating signal magnitude to force as well as percent crosstalk between components are summarized in Table 3.1.

CHAPTER IV

EXPERIMENTATION

Collection of data from the complete system can be divided into three principal areas. These areas are:

1. The load versus traction characteristics of the tape at high and low speeds.

2. The nominal (long time constant) temperature versus load for high and low speed.

3. The transient temperature response of the system under various load, speed and start-stop conditions.

Each of these topics will be discussed in terms of experimental procedure, the results, implications and conclusions.

TRACTION VERSUS LOAD MEASUREMENTS

The traction versus load data are presented in Figure 4.1. Analysis of the graphs indicate one traction regime for the low speed and two traction regimes for the high speed experiments. The low speed traction versus load curve is due to direct tape-head contact. The high speed measurements were divided into two regimes; (1) non-contact hydrodynamic film region, and (2) tape-head contact region. The traction versus load curve enables the estimation of film thickness subsequently an approximate film thickness for the hydrodynamic film breakdown. The following analysis presents a first order computation of these quantitites. [See Figure 4.2]

For a Newtonian fluid

$$\tau_H = -\mu \left.\frac{\delta u}{\delta y}\right|_{y=n} \qquad (4.1)$$

where

$\tau_H \equiv$ shear stress on tape head

$\mu \equiv$ kinematic viscosity

$\frac{\delta u}{\delta y}\Big|_{y=h}$ = slope of velocity profile at tape head

The film velocity profile can be approximated by a linear model

$$V_{AIR} = - \frac{v_s}{h} y + v_s \qquad (4.2)$$

where

V_{AIR} = velocity of the air @ y

v_s = tape speed

h = film thickness

Upon differentiation

$$\frac{\delta V_{AIR}}{\delta y} = - \frac{v_s}{h} \qquad (4.3)$$

substituting into (4.1)

$$\tau_H = \mu \frac{v_s}{h} \qquad (4.4)$$

using the definition of shear stress

$$\tau_H = \frac{F_T}{A_c} \qquad (4.5)$$

where

F_T = traction force

A_c = film contact area

Estimating the film contact area as 1.5 times the direct contact area

$$A_c = 1.5\ A_{DC} \qquad (4.6)$$

where

A_{DC} = direct contact area

upon substitution of (4.6) into (4.5) into (4.4) and solving for h

$$h = \frac{1.5\ \mu\ V_s\ A_{DC}}{F_T}$$

upon substitution of known values

=> μ_{AIR} @ 22°C = 1.82×10^{-5} Pa-s

v_s = 3.82 m/sec

$A_{DC} = \frac{15°}{360}\ 2\pi(0.8 \text{ inches})(0.5 \text{ inches}) = 68 \text{ mm}^2$

h = 7.1×10^{-6} mm/y or 6.3×10^{-8} in/x

where

Y = Traction Force in Newtons

X = Traction Force in lb_f

Table 4.1 displays the resulting film thickness for measured traction versus load data. The breakdown load is estimated from the traction versus load curve and then used to estimate the breakdown film thickness.

Based on the following analysis and using the estimate for breakdown traction (corresponding to breakdown load), the breakdown film thickness was computed to be 0.20 μm. The surface roughness perpendicular to the direction of running was measured using the Bendix type RLC Model 4 profilometer which uses a diamond stylus. The center line average for this surface was 0.05 μm for a cutoff length of 0.76 mm. However, the waviness of the surface was approximately 0.20 μm based on a total sample length of 6mm. These measurements correspond to approximately the breakdown film thickness and therefore a causal relationship is implied. A sample total surface profile taken along the centerline of the sapphire tape head in a direction perpendicular to the running direction is displayed in Figure 4.3.

TEMPERATURE MEASUREMENTS

The temperature measurements were made under various conditions in either the steady state or transient mode. In either case, all measurements were taken at the center of the contact region (Figure 4.4).

In order to compute the temperatures corresponding to particular signal strengths, the operating equation for this particular configuration must be obtained. This derivation was performed in Appendix A and will be quoted here. For direct tape contact the operating equation is

$$S = K'' \left[\rho_s N_E + (1 - \rho_s)^2 N_E \tau^2 \rho d_T + \varepsilon_T (1 - \rho_2) t N_T - N_E\right] . \qquad (7.11)$$

For a non-contact film, the operating equation is (Appendix A)

$$S = K'' \left[\rho_s N_E + (1 - \rho_s)^4 N_E \tau^2 \rho d_T + \varepsilon_T (1 - \rho_s)^2 \tau N_T - N_E\right] . \qquad (7.12)$$

The application of these equations can be greatly simplified by using the fact that at the start of each measurement the tape is at the ambient temperature. Thus the rise above the

ambient temperature can be found by noting the initial signal and measuring all other signal from this reference. For direct contact, the operating equation becomes

$$\Delta s = K'' \left[(1 - \rho_s)^{\tau} \varepsilon_T \{ N_T(T_o) - N_T(T_{AMB}) \} \right] .$$

This equation may be used as viewing a surface with effective emissivity of $(1 - \rho_s)^{\tau} \varepsilon_T$. Table 4.2 displays the numeric values for tapes 1 and 2* ($\varepsilon_T = 0.8$).

STEADY-STATE TEMPERATURE MEASUREMENTS

The first set of results displays the average or steady-state temperature of the tape under various load and speed conditions. Table 4.3 summarizes the experiments performed.

The high speed data correlated qualitatively with the traction versus load curve. Small temperature rises are observed in the hydrodynamic film region while much higher temperature rises are observed in the direct contact region. The actual data in load, traction, and temperature for one high speed run is shown in Figure 4.5. The direct contact effective emissivity is used in constructing the temperature scale. [only a 7% difference from non-contact effective emissivity]. The reader should note that over this small temperature interval the signal has nearly a linear relation with temperature (Appendix B). The low speed data displays an approximate linear variation of temperature with load as expected from the traction versus load curve as shown in Figure 4.1.

TRANSIENT TEMPERATURE MEASUREMENTS

The third set of experiments were designed to observe temperature transients at the sapphire tape-head magnetic tape interface. The primary consideration for detecting such a transient is to minimize the noise level in the signal while retaining the ability to detect temperature transients at the limit of the response of the detector. Because noise is proportional to the bandwidth to the one-half power, a high-low pass filter with minimum bandwidth can greatly increase the sensitivity of the RM2A in the AC-mode. The following criteria were used to set the limits on the high and low pass filter.

LOW PASS FILTER SET

The low pass filter must be set at a high enough frequency

*Only tapes 1 and 2 were used for temperature measurements for ease of computation.

to allow the fastest response of the system. By setting the low pass limit at the frequency corresponding to one quarter of the period of the defector rise time, all frequencies below the highest frequency possible will be passed. Designating F_i to equal the low pass frequency set, this value is computed to be

$$f_L = \frac{1}{T} = \frac{1}{4(R.T.)} = \frac{1}{4(7.75)\mu sec)} = 32.3 \text{ kHz}$$

where

T ≡ period

R.T. = detector rise time

HIGH PASS FILTER SET

The lowest frequency which needs to be passed by the filter corresponds to the time duration of a possible hot spot. The time duration is the time that a hot spot, the size of the microscope spot size, would take to cross the microscope field of view. Designating f_H as the frequency of the high pass filter, this value is computed to be

$$f_H = \frac{1}{T} = \frac{1}{2\Delta t} = \frac{V_T}{2(S.D.)}$$

where

T = period

Δt = time for the spot to cross the microscope field of view

V_T = tape speed

S.D. = spot diameter

Table 4.4 displays the numerical values of f_H for both high and low tape speeds and magnifications. By increasing f_H to the value of f_L, although the full signal duration will be reduced, the noise will be minimized. Table 4.5 displays the smallest detectable temperature rise in the A-C mode. This table also indicates the dramatic increase in sensitivity with filtering.

The following referred to figures are the actual output from the Barnes RM2A infrared microscope as recorded by the Nicolet digital oscilloscope. These figures display the noise levels in the unfiltered (Figure 4.6) and the filtered (Figure 4.7) signals.

Approximately 15 to 20 attempts to observe temperature transients were made at various loads and speeds but no detectable temperature transients were observed. In particular, a start/stop mode using a running load of 0.52N at low speed and a stop load of 1.68N created no measurable transients in excess of the signal noise.

THE AGA THERMOVISION 750

The AGA Thermovision 750 system was used to look at the overall radiation pattern of the tape-tape head contact and single line line scan was used at the center of the contact. The AGA was focused on the magnetic tape - sapphire tape head interface while the full scale adjustment was set for a 2°C Black body scale. This scale corresponds to a ~3°C scale for the tape. The darker areas correspond to areas emitting relatively less radiation. The video display of the slow speed under a 0.7N load is shown in Figure 4.8.

The darker region within the contact displays a loss of radiation due the specular reflectivity as in the radiation analysis for the Barnes system. The dark contact region also shows that the temperature rise within the contact must be less than 3°C as observed with the Barnes system. Graduations of temperature cannot be seen very well, since at this low temperature range the image produced by the AGA system is essentially binary. The AGA system also indicated that there are no substantial temperature fluctuations over the contact region.

CHAPTER V

CONCLUSIONS

The temperature increases in the steady state mode over the range of load and speed were on the order of a few degrees centigrade. The temperature flashes, if they exist, were determined to be less than ~10°C. Dependent upon the largest acceptable temperature rise, further studies should concentrate on temperature rises over longer periods of running time in the steady state mode and/or the construction of specialized filters which could lower the minumum detectable temperature rise in the transient mode. These measurements should be made over a more typical range of loads to remove the possibility of tape delamination and severe deformation.* Also, the reduction of spot size and increase in minimal detectable temperature does not warrant the continued use of the 36x objective.

One possible explanation of the lack of temperature flashes of sufficient magnitude to be measured can be found by a qualitative analysis of the asperity interaction which may cause them. The tape head has an almost optically smooth surface and because the tape is so thin (1 thousandth of an inch) and has a relatively low modulus of elasticity, any asperity interaction between the surface and head would cause the tape to assume a planar orientation. Thus such a thin tape would conform to the tape head surface without sufficiently high local stresses to cause a measurable temperature flash.

Although not required by this contract the traction versus load characteristics of the tape head were measured. The high speed measurements were divided into two regions:

1. non-contacting hydrodynamic film region
2. tape-tape head contact region.

Further exploration into the effects of tape tension, speed and tape head surface roughness could lead to useful results in creating low temperature producing hydrodynamic film within the tape head-magnetic tape interface.

*During experimentation the low rigidity of the magnetic tape, slight curvature of the low friction rollers, and high tape tension produced sporatic tape deformation and determination.

REFERENCES

1. AGA Infrared Systems, AGA Thermovision 750 Operating Manual, Publication 556-103 612, Lindingo, Sweden (1976).

2. Barnes Engineering Company, Instruction Manual Infrared Radiometric Microscope Model RM-2A, Stamford, Connecticut (1975).

3. Siegel, Robert and Howell, John R. *Thermal Radiation Heat Transfer*, 2nd Ed. Washington: Hemisphere Publishing Co., McGraw Hill Book Co. (1981).

4. Union Carbide, Technical Bulletin: Optical Properties and Applications of Linde Cz Sapphire, Copyright F-CPD 72950, San Diego, California (1972).

APPENDIX A

The following radiation analysis for the Barnes RM-2A infrared microscope applies the basic operating equation to particular geometries and operational modes which will prove useful in this research effort.

Basic Operating Equation

$$S \alpha \Delta Q$$

where

S = signal output

ΔQ = the difference in the radiation between the chopper and target arriving at the detector

Let

= proportionality constant

$$S = K \Delta Q$$

$$= K \Delta Q'' A_D \Delta \Omega$$

$$= K' \Delta Q''$$

where

K' = modified proportionality constant ($= K A_D \Delta\Omega$)

A_D = area of detector

$\Delta\Omega$ = solid angle over which there is change in radiation flux

$\Delta Q''$ = difference in radiation per unit area per unit solid angle

Explicitly

$$\Delta Q'' = Q''_{T-D} - Q''_{C-D}$$

where

Q''_{T-D} = radiation flux per unit steradian from the target arriving at the detector

Q''_{C-D} = radiation flux per unit steradian from the chopper arriving at the detector

These radiative flux terms may be written in more detail by denoting the origin of the radiation.

$$Q''_{T-D} = \varepsilon_T N_T F_{T-D} + \rho_{d_T} N_E^* + \rho_{S_T} N_E F_{O(T) - D} \qquad (A.1)$$

$$Q''_{C-D} = \varepsilon_C N_C F_{C-D} \qquad (A.2)$$

where (in generalized notation)

F_{A-B} = the fraction of radiation from surface A arriving at surface B

N_A = the blackbody emissive power per unit steradian of body A at temperature, T_A (watts/cm^2 steradian)

ε_A = emissivity of surface A

ρ_{d_A} = diffuse reflectivity of surface A

ρ_{s_A} = specular reflectivity of surface A

subscripts

T = target

C = chopper

E = environment

O(T) = objective imaged by the target surface

superscripts

quantity* $\equiv$ effective quantity

The primary assumptions behind these equations are

1. the objective surface (facing the target surface) radiates as a blackbody at the environmental temperature

2. the environment radiates as a blackbody at the environmental temperature

Given that the chopper has an emissivity of 1, [$\varepsilon_C = 1$], and is at the environment temperature, T_ε, then

$$Q''_{C-D} = N_E F_{C-D} \quad . \tag{A.3}$$

Since the chopper blocks the same solid angle that the objective uses to send the radiation collected from the target to the detector, the corresponding shape factors are equal. That is

$$F_{C-D} = F_{T-D} \quad . \tag{A.4}$$

Upon substitution of equations 1, 2, 3, and 4 into the operating equation

$$S = K' \left[\varepsilon_T N_T F_{T-D} + \rho_{d_T} N_E^* F_{T-D} + \rho_{S_T} N_E F_{O(T)-D} - N_E F_{T-D}\right] .$$

By factoring F_{T-D} outside the brackets

$$S = K''\left[\varepsilon_T N_T + \rho_{d_T} N_E^* + \rho_{S_T} N_E \frac{F_{O(T)-D}}{F_{T-D}} - N_E\right] \tag{A.5}$$

where K" = twice modified proportionality constant.

The Factor $F_{O(T)-D}$ will be evaluated for two specific geometries. First it will be evaluated when focused on the target surface, and next when the objective is at half the working distance.

Case I. At full focus distance (Figure A.1)

Since the image of the objective surface can only radiate back to those same surfaces, and therefore not into the acceptance cone of the objective, then no radiation can be specularly reflected from the surroundings to the detector. Thus

$$F_{O(T)-D} \cong 0 \quad \text{at focus}$$

Upon substitution into equation (A.5)

$$S = K'' [\varepsilon_T \cdot N_T + \rho_{d_T} N_E^* - N_E] \qquad (A.6)$$

Case II at half working distance (Figure A.2)

At half the working distance, the image of the objective surface radiates fully into the acceptance cone of the objective. Thus

$$F_{O(T)-D} = F_{T-D}$$

Upon substitution into equation (A.5)

$$S = K''[\varepsilon_T N_T + \rho_{d_T} N_E^* + \rho_{S_T} N_E - N_E] \qquad (A.7)$$

The diffuse reflectivity represents the fraction of radiation, incident at all angles to the surface, from the environment which is uniformly reflected back to the environment. The objective mirror does not radiate any energy in the infrared band of interest and reflects onto the surface only that radiation emitted from the detector. Since the detector is at 77°K, it emits relatively no radiation. Thus the mirror contributes no radiation to the surface and subsequently must have its contribution subtracted off from the radiation which would arrive from the environment acting as a black body over a hemisphere around a point on the surface. In this way, the true or effective environmental radiation arriving at the surface subject to diffuse reflection is found. In order to adjust N_E the amount of radiation from the environment to the spot within the acceptance cone of the objective must be computed [Q''_{E-T}]. This calculation is independent of the distance between the target and objective since the formulation is based upon solid angles. Referring to Figure A.3.

$$Q_{E-T} = N_E(F_{\infty-T} A_\infty + F_{I-T} A_I - F_{II-T} A_{II})$$

where

A_∞ = Area of infinite palen

A_I = Area of circle I

A_{II} = Area of circle II (Imaginary surface)

Using reciprocity relation

$$F_{B-C}\, A_B = F_{C-B}\, A_C$$

$$Q_{E-T} = N_E\, (F_{T-\infty}\, A_T + F_{T-I}\, A_T - F_{T-II}\, A_T)$$

$$\frac{Q_{E-T}}{A_T} = N_E\, (F_{T-\infty} + F_{T-I} - F_{T-II})$$

From Reference 3

$$F_{T-I} = \frac{R_I^{\,2}}{h_I^{\,2} + R_I^{\,2}}$$

$$F_{T-II} = \frac{R_{II}^{\,2}}{h_{II}^{\,2} + R_{II}^{\,2}}$$

$$F_{T-\infty} = 1.0$$

Numerical results for $Q"_{E-T}$ (N_E^*) for each objective is present in Table A.1.

The only factor left unknown is K" which will be called the calibration constant, since its value will be determined from experiment. If the infrared microscope is viewing a black body source, equation A.5 becomes

$$S = K" \, [N_T - N_E] \qquad (A.8)$$

Thus K" can be computed by measuring the temperature of the environment and the black body source. Table A.2 displays the numeric values of K" for each objective in both D.C. (steady-state) and A.C. (transient) nodes.

Using the results of N* for the 15x objective and making use of Kirchoff's Law, equations (A.6) and (A.7) for the output at focus and one-half the working distance may be written as

At focus

$$S_F = K" \left[\varepsilon_T(N_T - N_E) - 0.12\, \rho_{d_T} N_E - \rho_{S_T} N_E\right] \qquad (A.9)$$

At one-half the working distance

$$S_{1/2} = K" \left[\varepsilon_T(N_T - N_E) - 0.12\, \rho_{d_T} N_E\right] . \qquad (A.10)$$

These results will be used extensively in the determinate of the tape radiative properties.

Although these equations apply equally to both the steady state and transient modes, they have been developed for a flat surface with no intervening media. An additional radiation analysis must be completed for the tape-tape head configuration so that temperatures may be related to radiation signals. The following ray diagram, Figure A.4, will greatly aid in this analysis.

Radiation can enter the acceptance cone of the objective from four sources, neglecting double reflections.

	Source	Contribution
1.	Radiation from the environment reflected from the top surface	$\rho_s N_E F_{T-D}$
2.	Radiation passing through the top surface and then reflected from the bottom surface diffusely	$(1-\rho_s)N_{ENV}\tau\rho_{d_T}\tau(1-\rho_s)F_{T-O}$
3.	Radiation emitted by tape	$\varepsilon_T N_T \tau (1-\rho_s)F_{T-D}$
4.	Radiation emitted by sapphire	$\varepsilon_s N_s \tau(1-\rho_s)F_{T-D}$

where

ρ_s = reflectivity of sapphire

τ = internal transmittance of sapphire for the thickness of the tape head

These contributions are correct when the Barnes unit is focused. Because all measurements will be made at focus, to obtain the smallest spot size, no other configurations will be discussed. The contribution from emission of the sapphire may be omitted upon examination of the sapphire radiative properties (Table A.3)

Since the heated region of the sapphire tape head will be very thin, the contribution due to the sapphire emission will be ignored. Upon substitution into the basic operation equation

$$S = K'' \left[\rho_s N_E + (1-\rho_s)^2 N_E \tau^2 \rho_{d_T} + \varepsilon_T (1-\rho_2)\tau N_T - N_E\right] \quad (A.11)$$

When an air film is present between the sapphire tape head and the magnetic tape the working equation will be slightly modified to the following form.

$$S = K'' \left[\rho_s N_E + (1-\rho_s)^4 N_E \tau^2 \rho_{d_T} + \varepsilon_T (1-\rho_s)^2 \tau N_T - N_E\right] \quad (A.12)$$

These equations will prove to be very useful in the analysis of experimental measurements.

APPENDIX B

Figure B.1 relates the effective black body radiance to temperature for the Barnes RM2A infrared microscope. The graph is obtained by numerically integrating, with respect to wavelength, the detector response curve over the black body curve for a specific temperature.

Table 2.1 TABULATION OF SIGNIFICANT PARAMETERS IN SPOT SIZE INCREASE DUE TO SAPPHIRE TAPE HEAD

Objective	t (inches)	F (inches)	F'(F+ζ) (inches)	D (inches)	D_1 (inches)	D_2 (inches)	n_1 (inches)
15x	0.16	0.95	1.01	0.75	0.0014	0.0049	1.67
36x	0.16	0.315	0.38	0.23	0.0007	0.0034	1.67

Table 2.2. Average response times for A.C. mode rise time and decay time; and D.C.-mode with narrow filter rise time

Response Measured	Average Response Time (seconds)
AC - rise time	7.75×10^{-6}
AC - natural decay	4.58×10^{-2}
DC - narrow filter rise time	0.51

Table 2.3 Tape Radiative Properties Nominal Values

Tape	ε_T	ρ_{DT}	ρ_{ST}	τ
1	0.80	0.10	0.10	0.0
2	0.80	0.11	0.09	0.0
3	0.86	0.06	0.08	0.0

Table 3.1. Tape Speeds

Rewind (high)	3.82 m/sec
Reverse (low)	0.32 m/sec

Table 3.2. Calibration of Triaxial Transducer

	Signal/Unit Force	Numeric Value for Crosstalk	Percent Crosstalk
Normal Load	458 mV/N_{load}	12 $mV/N_{Traction}$	2.6
Traction	458 $mV/N_{Traction}$	12 mV/N_{load}	2.6

Table 4.1. Film Thickness as a Function of Traction Force

h (μm)	Traction (N)	Load (N)	
0.79	0.009	0.25	
0.47	0.015	0.50	
0.36	0.020	0.75	
0.27	0.026	1.00	
0.23	0.031	1.25	
0.20	0.036	1.50*	Breakdown Load

*Breakdown load as estimated from the traction versus load curve.

Table 4.2. Tape Effective Emissivity

Direct Contact	0.70
Non-Contact Film	0.65

Table 4.3. Temperature Measurement in Steady State Mode
(15x Objective)
Instrument Response Time 0.51 seconds

Tape Running Conditions			Measured Temperature	Error
Speed (m/s)	Load (N)	Run Time (minutes)	Rise Above Ambient (°C)	Interval
3.82	0.7*	0.5	0.0	0.6
3.82	1.1*	0.3	0.5	0.6
3.82	2.4*	0.5	3.2	0.5
3.82	2.6*	0.5	3.5	0.5
0.32	0.6	1.0	0.4	0.5
0.32	1.2	1.0	1.0	0.5
0.32	1.7	1.0	1.1	0.5

* measured at peak load at the end of the load transient
non-contact film region
this scan displayed in Figure 4.5

Table 4.4. High pass filter setting for magnification and tape speed

	f_H (kHz)
(36x, 3.82 m/s)	22.1
(36x, 0.32 m/s)	1.9
(15x, 3.82 m/s)	15.3
(15x, 0.32 m/s)	1.3

Table 4.5. Minimum Detectable Temperature Rise above Ambient as Computed for each Objective

Objective	*Minimum detectable temperature rise above ambient (°C) ΔT	
	Triangular Filter (32.3 kHz)	No Filter
36x	13	90
15x	9	90

* ΔT was computed in the same manner as the temperature error interval explained in Chapter II

Table A.1. Values of the effective environment radiation for diffuse reflection

OBJECTIVE	N_E^*
15x	0.88 N_E
36x	0.92 N_E

Table A.2. Calibration Constants

Objective	$K''_{D.C.}$ [millivolts/milliwatt/cm^2-steradian]	$K''_{A.C.}$ [millivolts/milliwatt/cm^2-steradian]
15x	161.6	5.09
36x	112.2	3.53

Table A.3. Sapphire Radiative Properties (4.06mm thickness)*

τ	0.93	
ρ_s	0.063	
ε_s	0.0 →	0.1mm thickness
	0.11 →	3.2mm thickness

*Reference [4]

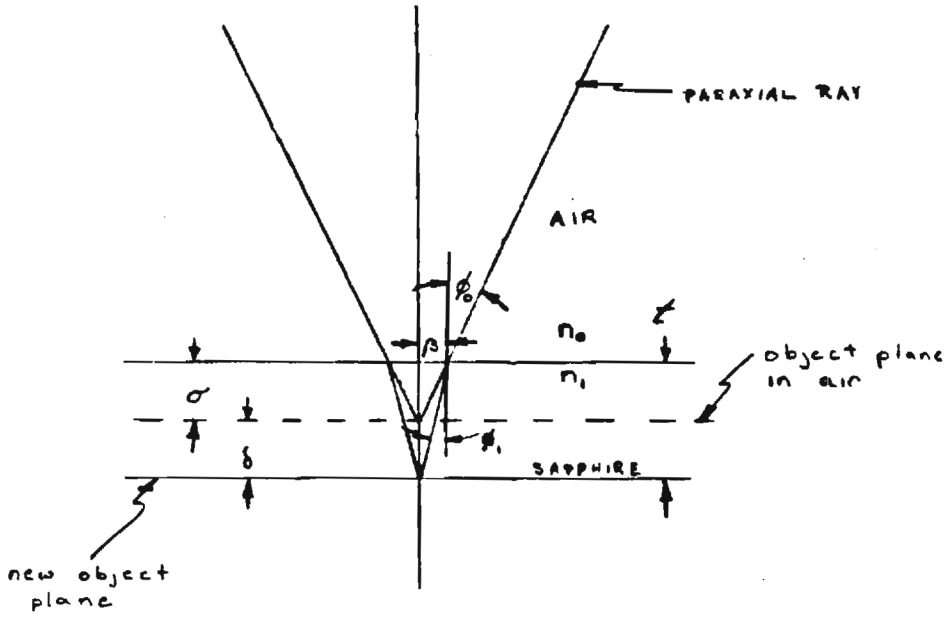

Figure 2.1 The shift in the object plane due to the presence of the sapphire tape head

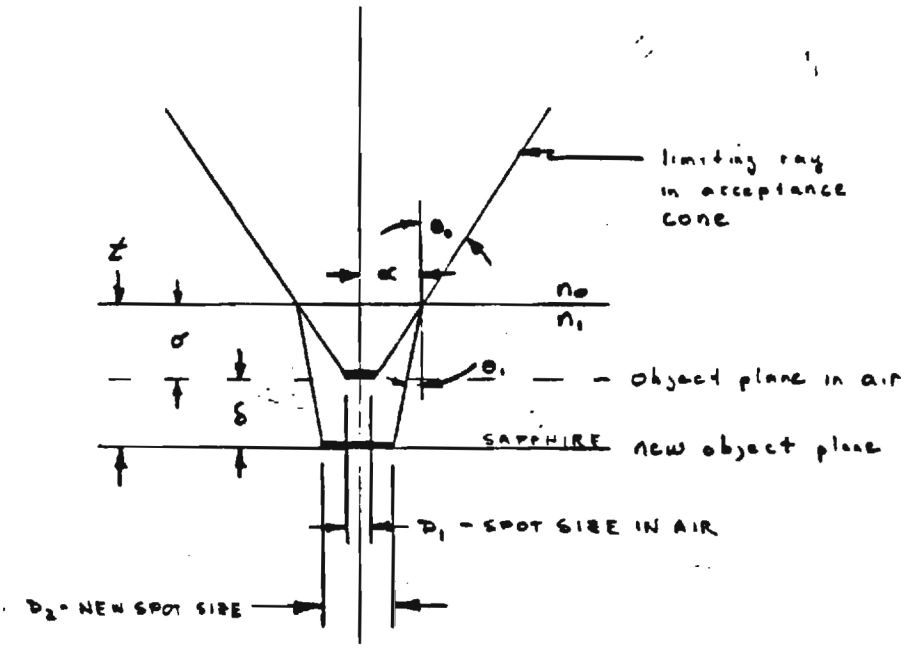

Figure 2.2 Spot size determination on sapphire surface contacting magnetic tape

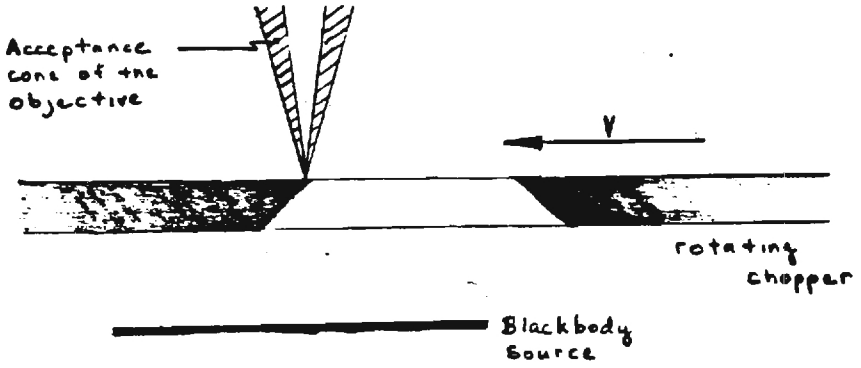

Figure 2.3 Rise time determination using rotating notched disk

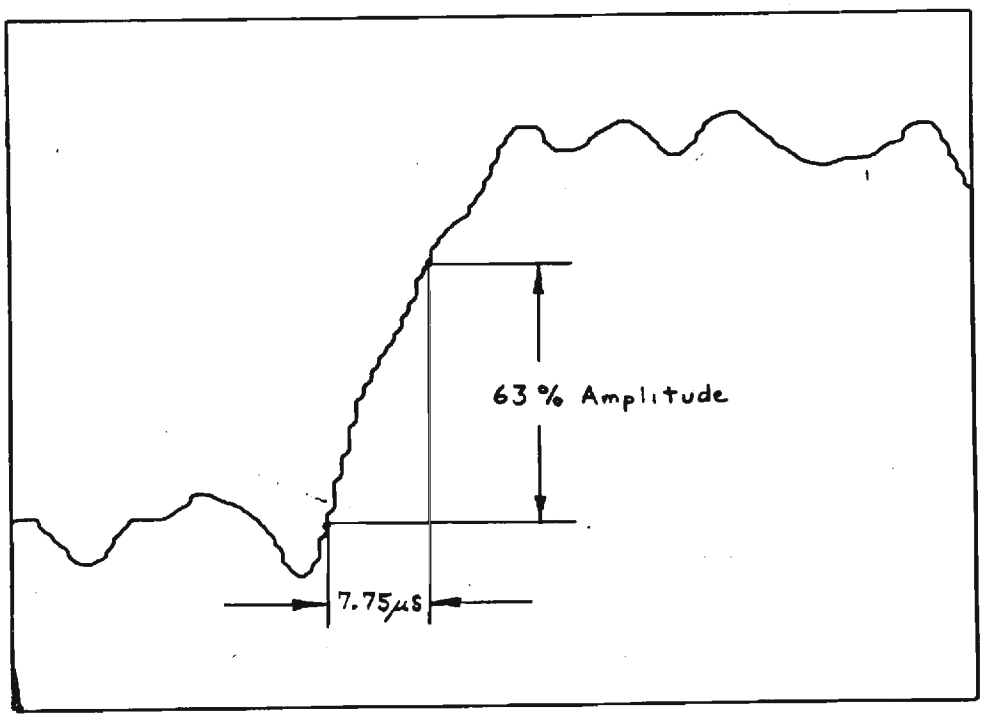

Figure 2.4 Actual scan of A-C mode displaying the measured rise time

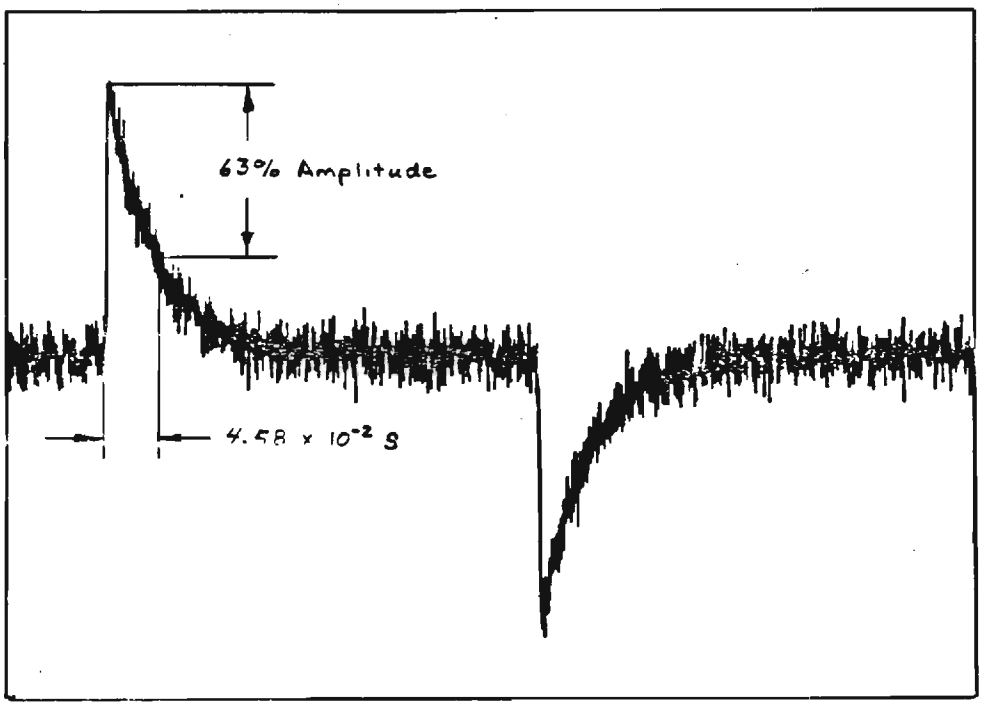

Figure 2.5 Actual scan of A-C mode displaying the measured decay time

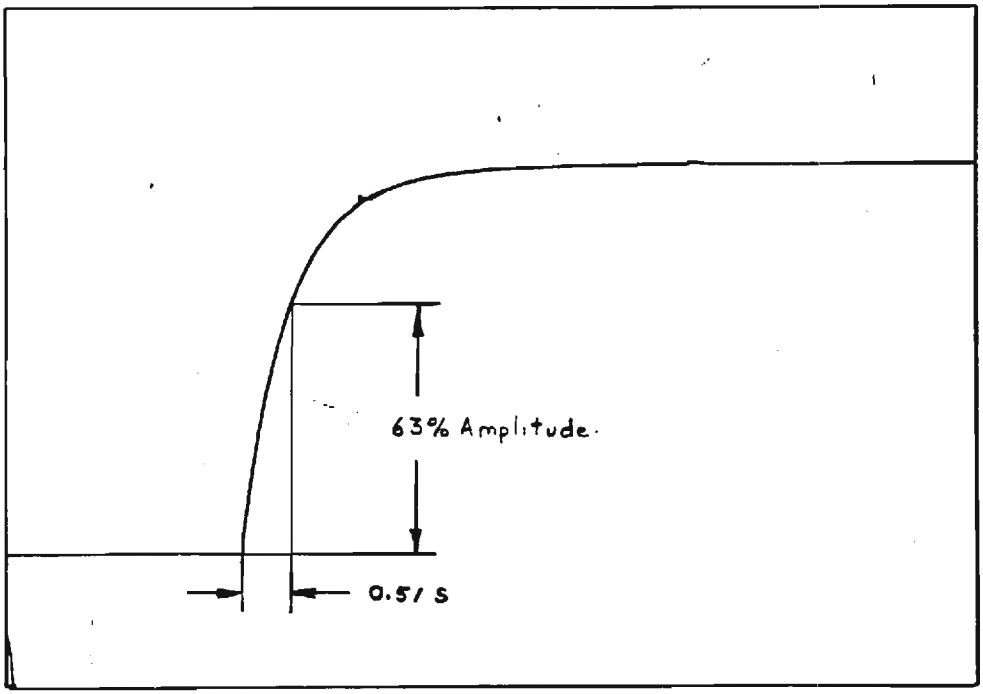

Figure 2.6 Actual scan of D-C mode with narrow filter displaying the measured rise time

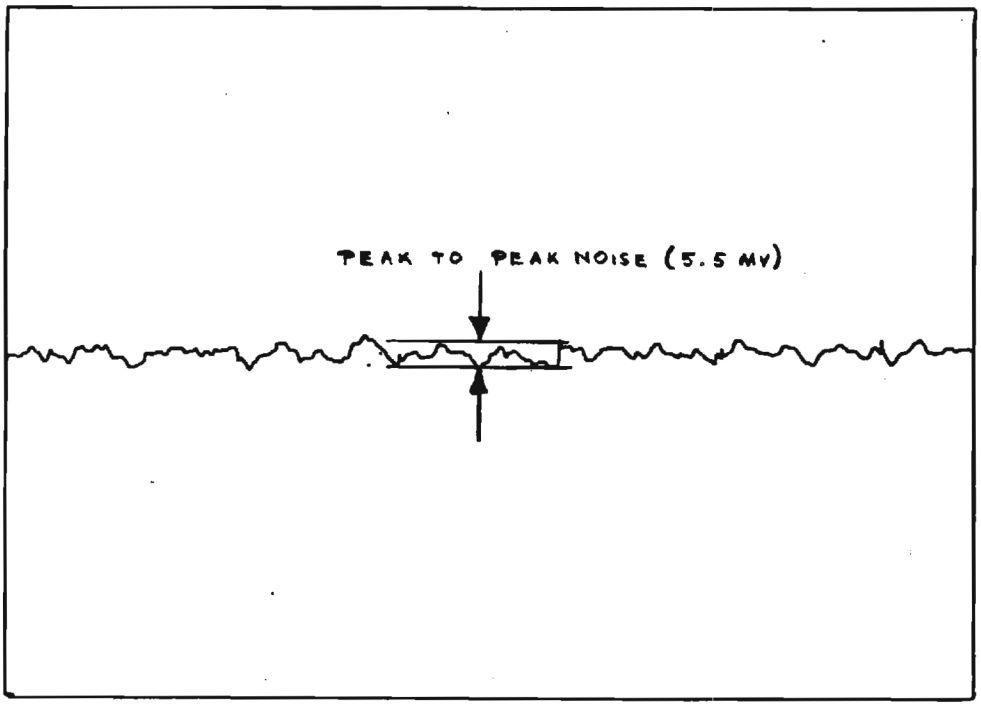

Figure 2.7 Actual scan of the signal in the D.C. mode with narrow filter while viewing a constant temperature source

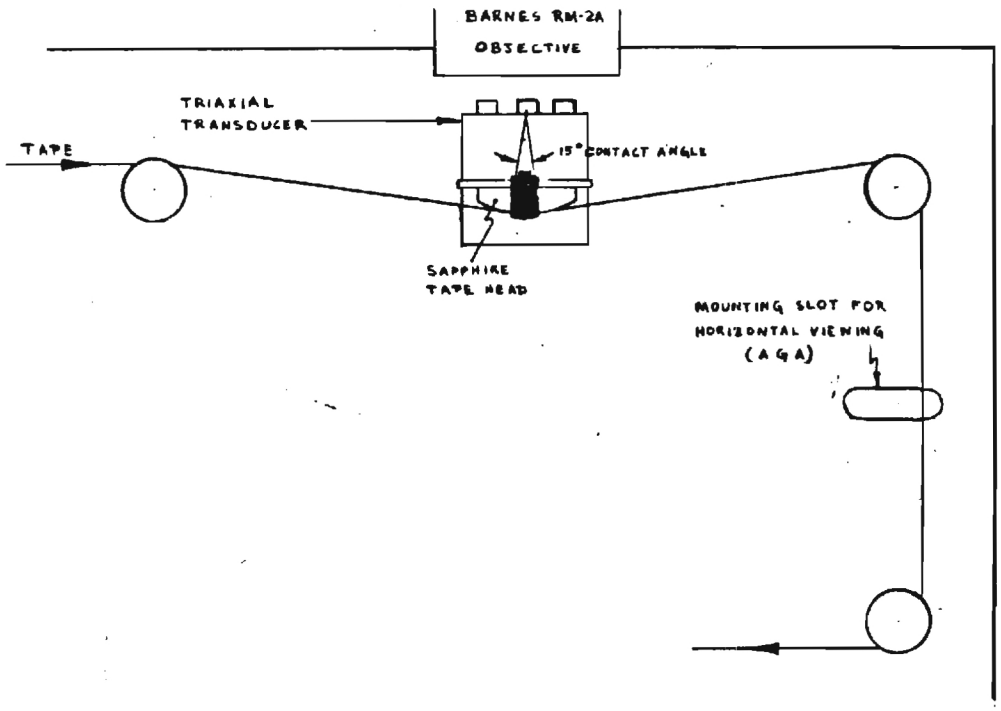

Figure 3.1 The tape transport system

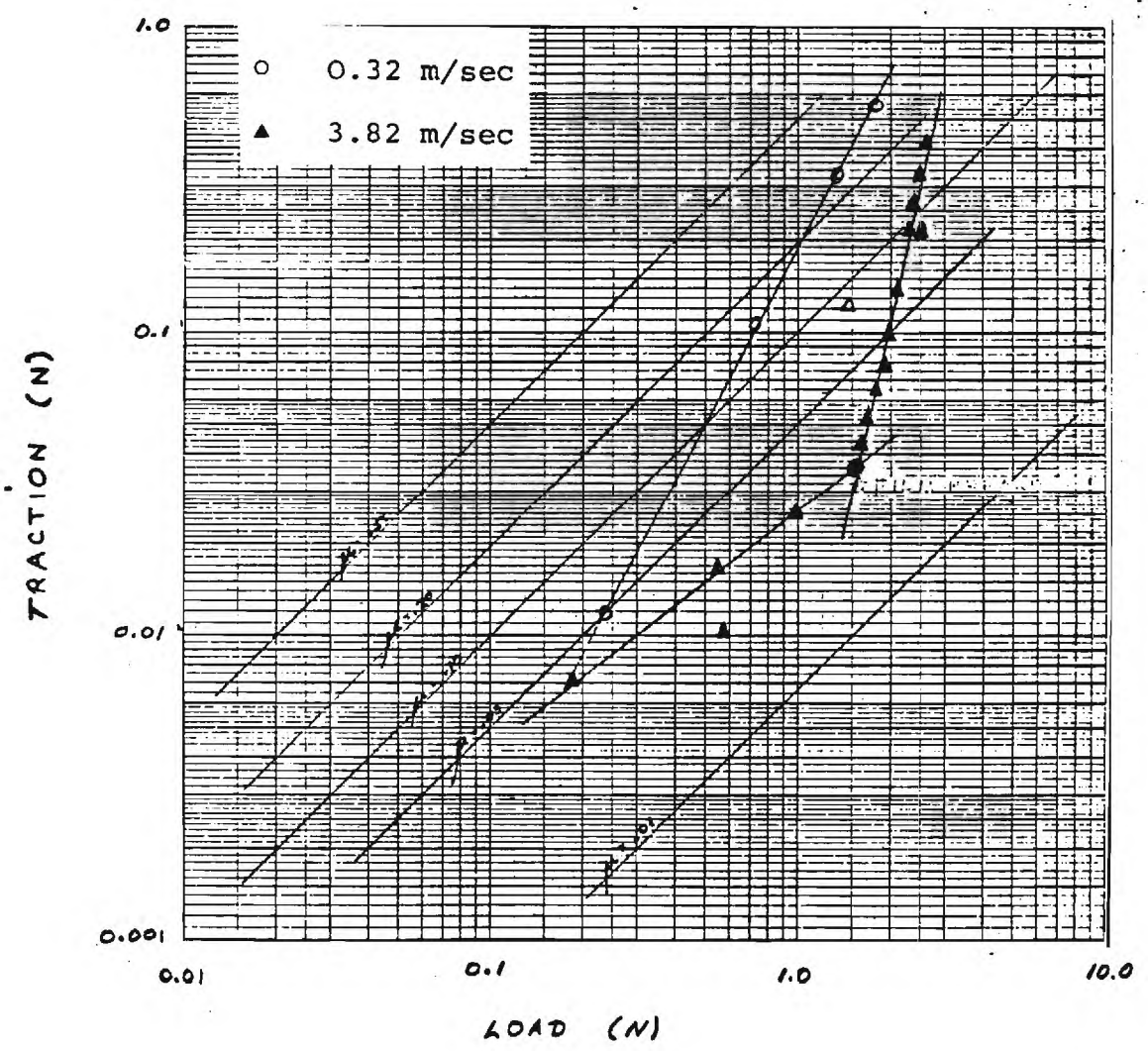

Figure 4.1 Traction vs load measurements at high and low speeds

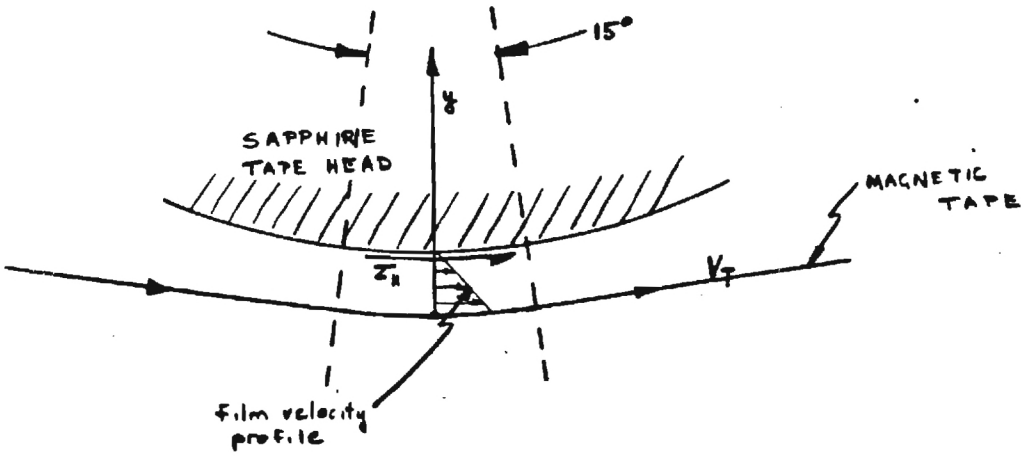

Figure 4.2 Assumed velocity profile in tape/tape head hydrodynamic film region

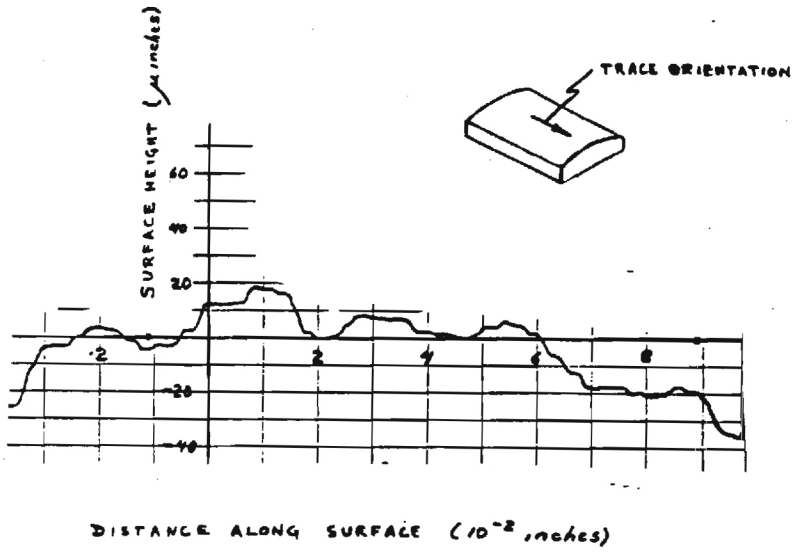

Figure 4.3 Total surface profile of the sapphire tape head

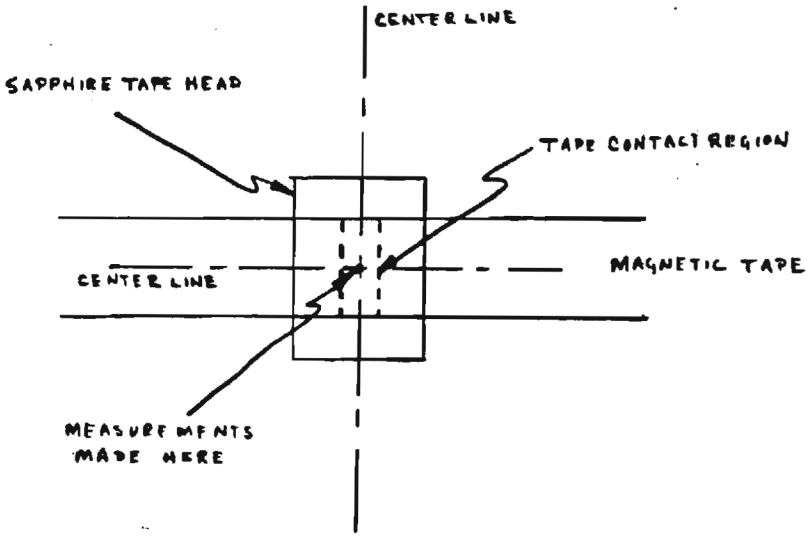

Figure 4.4 Position of the spot where temperature measurements were made

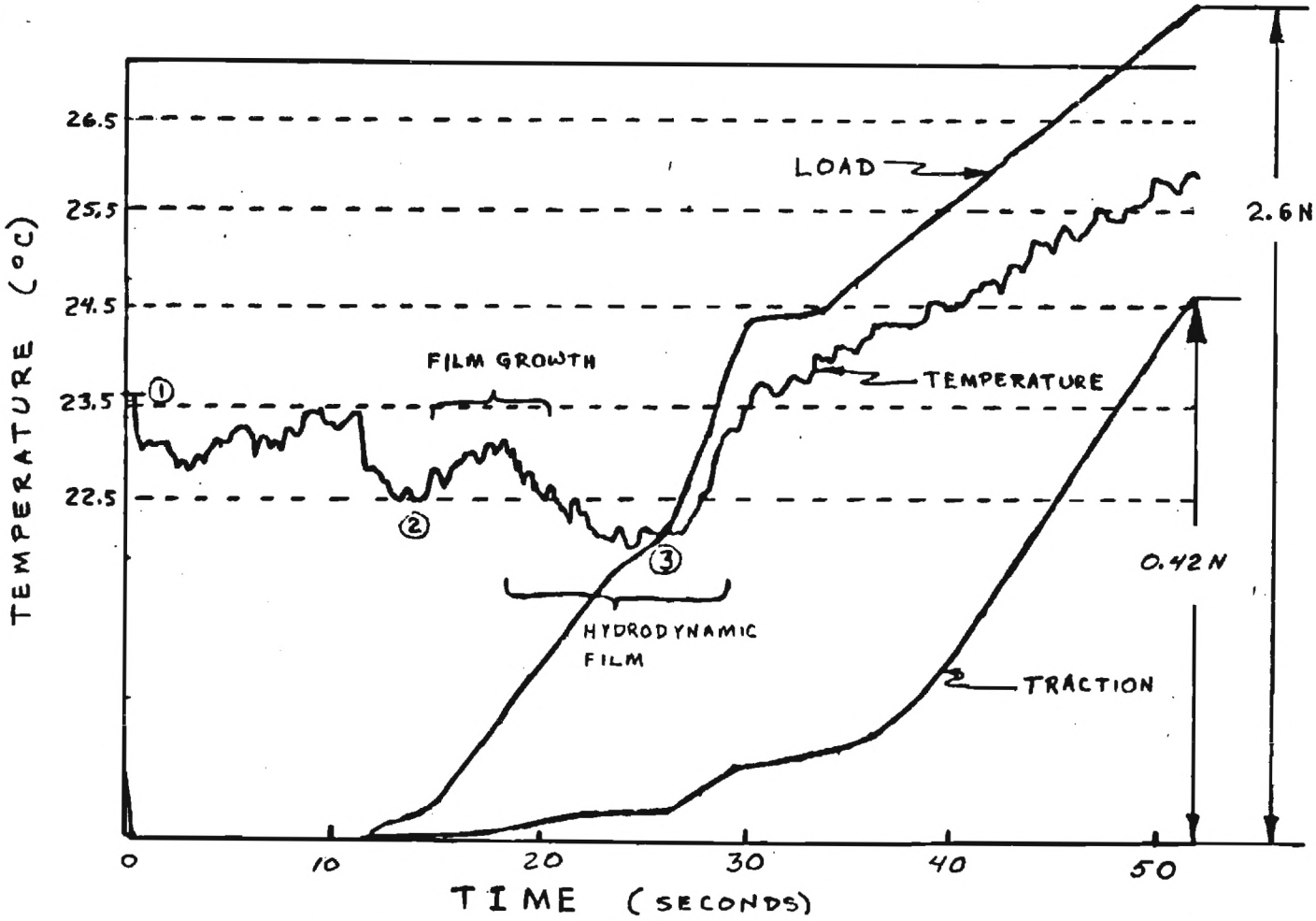

Figure 4.5 The traction, load and temperature versus time for one high speed load transient. Points 1, 2, and 3 mark the ambient temperature signal levels for a black body, direct film contact, and non-contact hydrodynamic film respectively

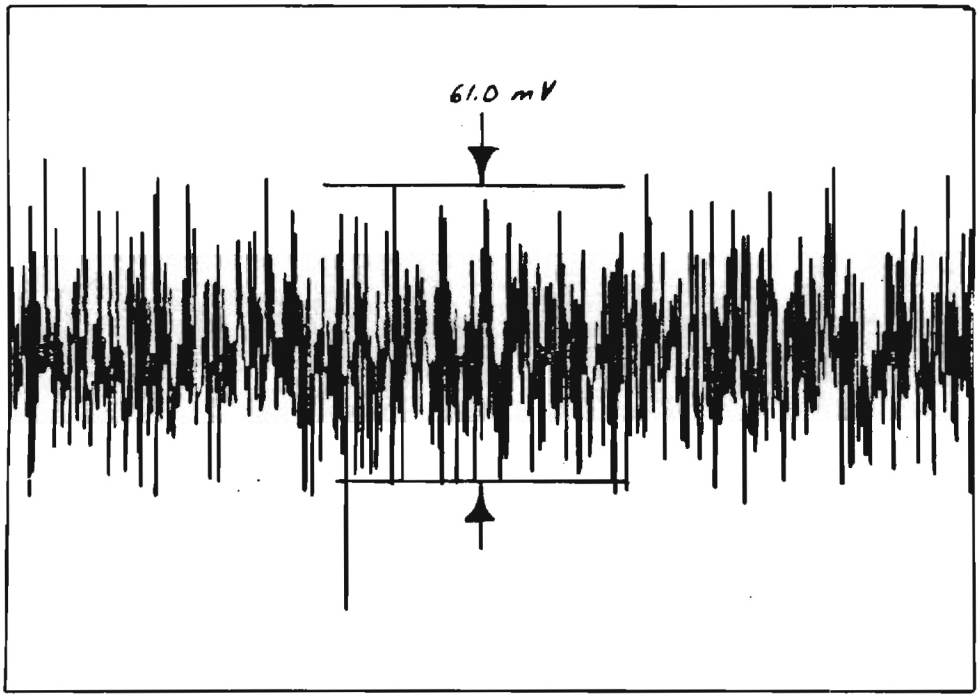

Figure 4.6 Noise level in an unfiltered A.C. mode scan

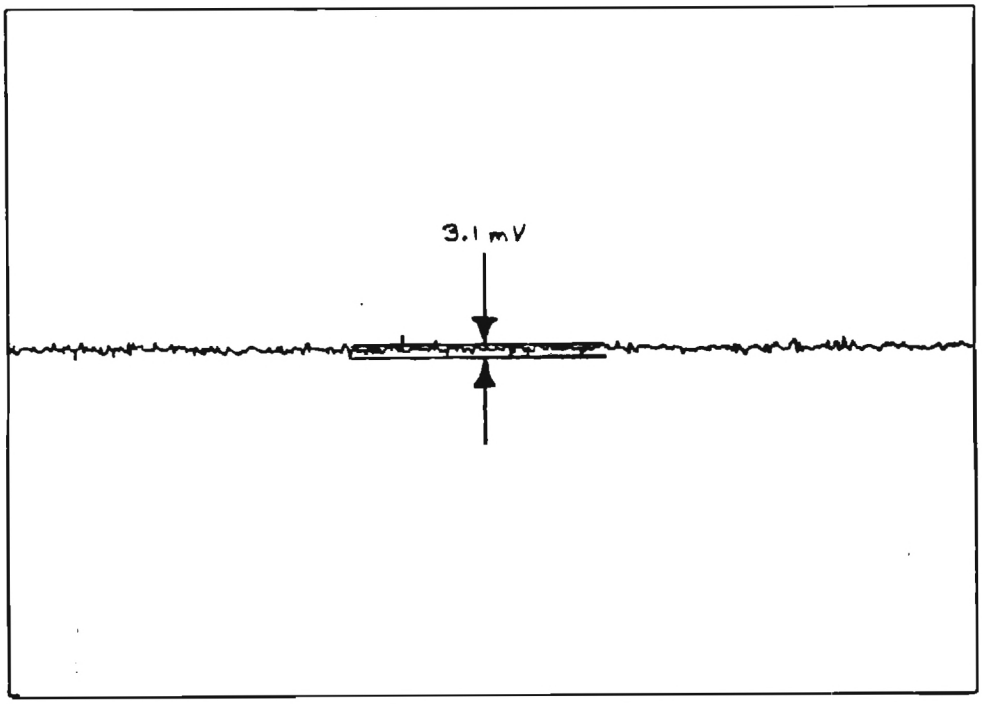

Figure 4.7 Noise level in a filtered A.C. mode scan

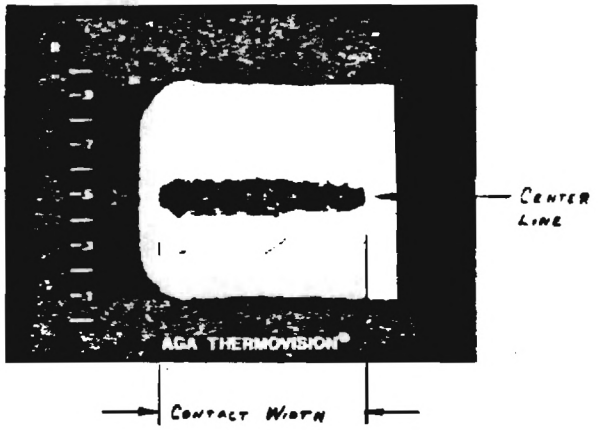

Figure 4.8 Video display of AGA Thermovision 750 while viewing tape/tape head interface at slow speed under a normal load of 0.7 Newtons

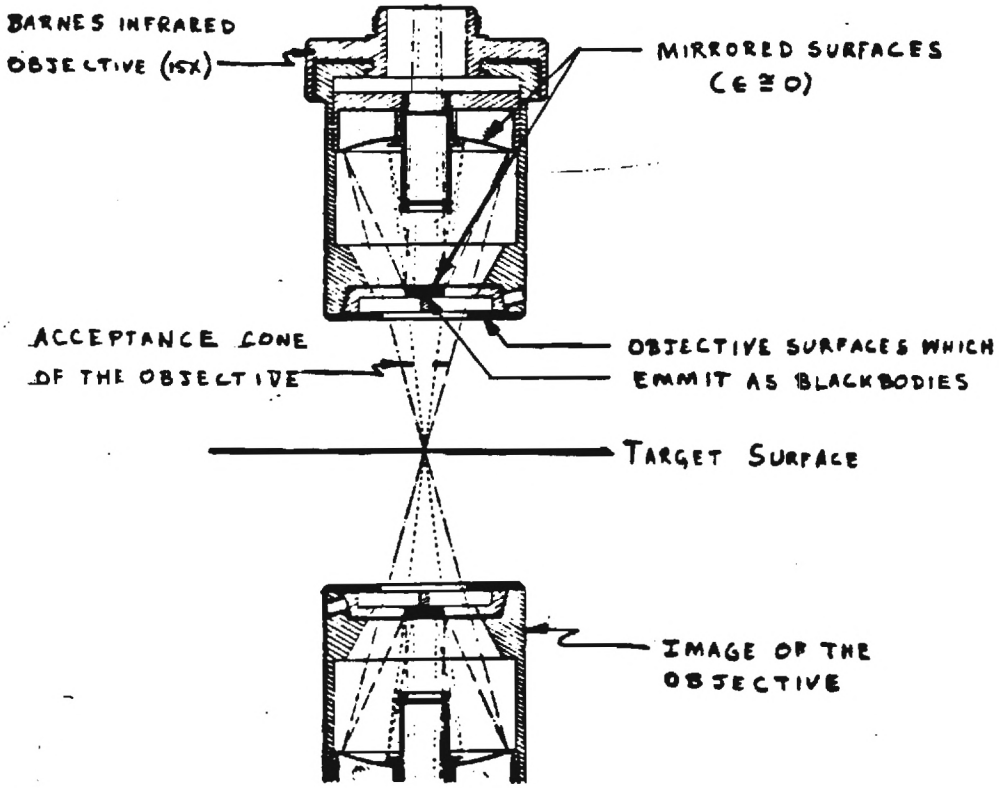

Figure A.1 Objective focused on target surface

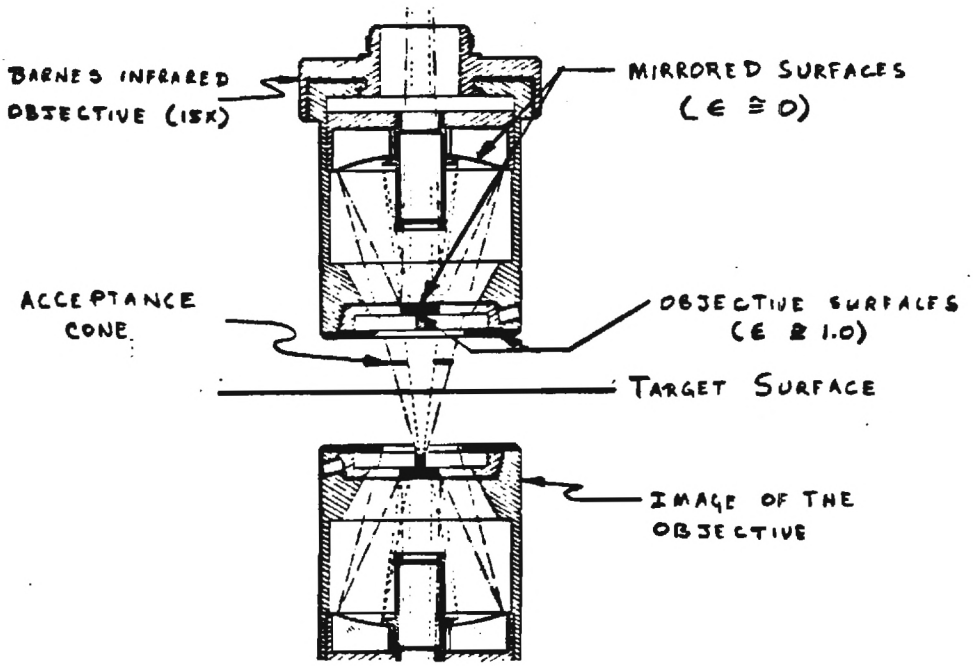

Figure A.2 Objective at half the working distance to the target

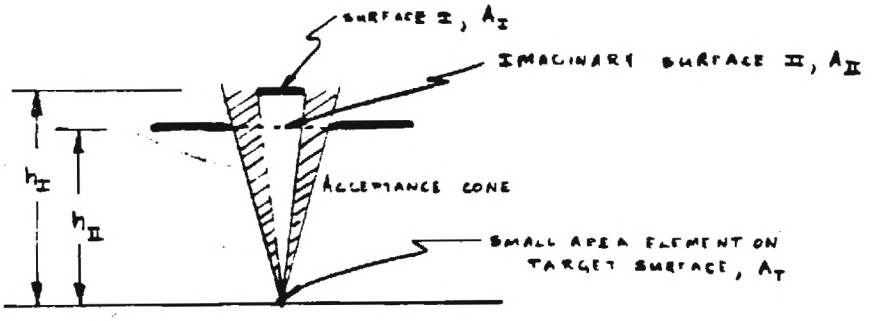

Figure A.3 Simplified geometry of the objective surface with respect to the target surface at focus

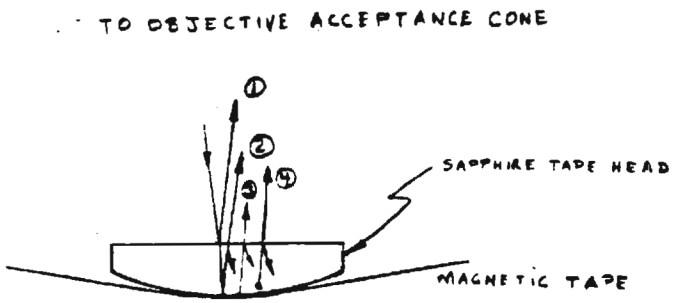

Figure A.4 Radiative contributions into objective acceptance cone

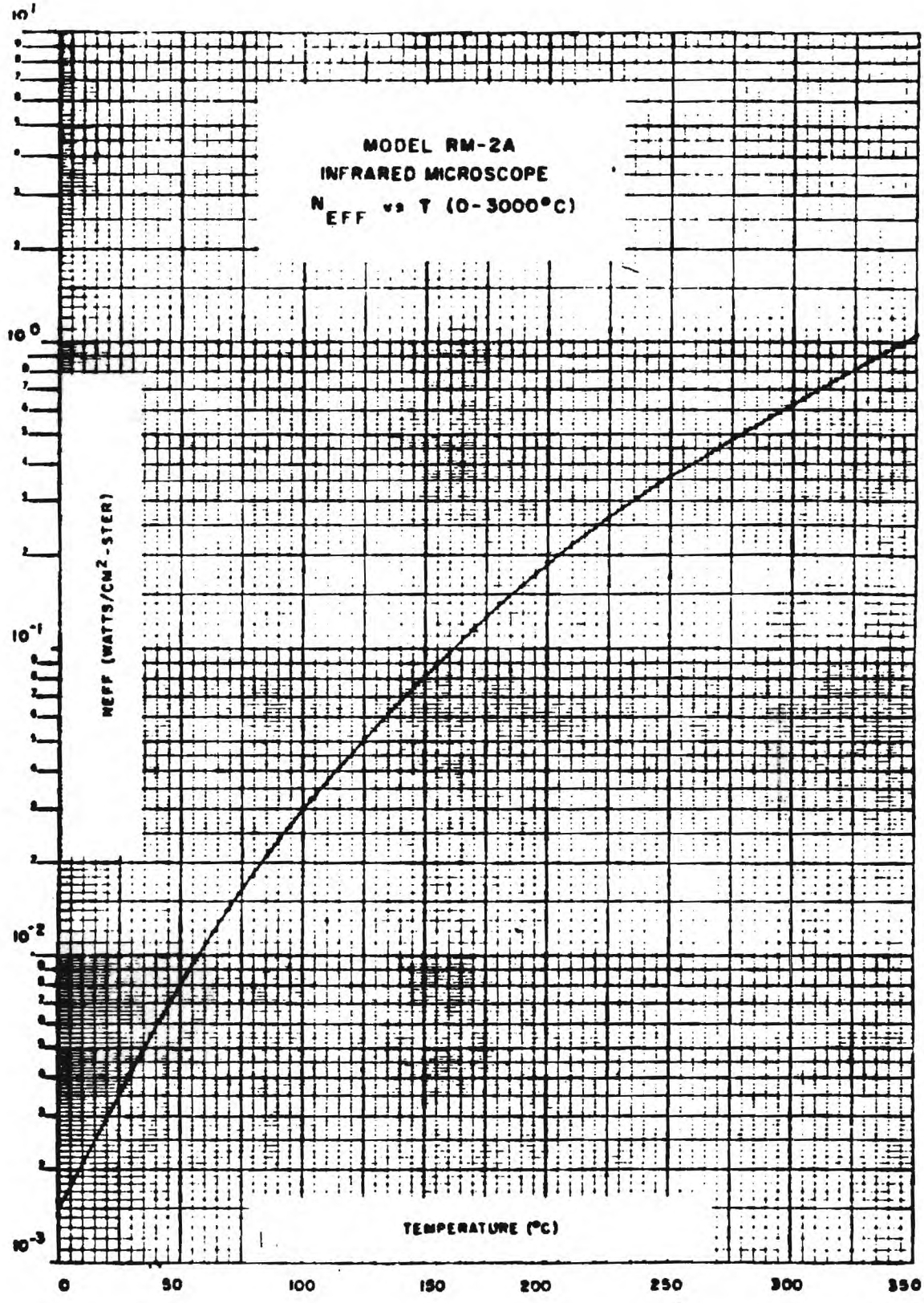

EFFECTIVE BLACKBODY RADIANCE vs. TEMPERATURE MODEL RM2A

Figure B.1 Effective black body radiance versus temperature model RM2A